ACS APPLIED MATERIALS & INTERFACES

Research Article

www.acsami.org

In Situ Cross-Linking of Stimuli-Responsive Hemicellulose Microgels during Spray Drying

Weifeng Zhao,[†,‡,§] Robertus Wahyu N. Nugroho,[†,§] Karin Odelius,[†] Ulrica Edlund,[†] Changsheng Zhao,[‡] and Ann-Christine Albertsson*[,†]

[†]Fiber and Polymer Technology, School of Chemical Science and Engineering, Royal Institute of Technology, Teknikringen 56-58, SE-100 44 Stockholm, Sweden

[‡]College of Polymer Science and Engineering, State Key Laboratory of Polymer Materials Engineering, Sichuan University, 610065 Chengdu, China

Supporting Information

ABSTRACT: Chemical cross-linking during spray drying offers the potential for green fabrication of microgels with a rapid stimuli response and good blood compatibility and provides a platform for stimuli-responsive hemicellulose microgels (SRHMGs). The cross-linking reaction occurs rapidly in situ at elevated temperature during spray drying, enabling the production of microgels in a large scale within a few minutes. The SRHMGs with an average size range of ∼1−4 μm contain *O*-acetyl-galactoglucomannan as a matrix and poly(acrylic acid), aniline pentamer (AP), and iron as functional additives, which are responsive to external changes in pH, electrochemical stimuli, magnetic field, or dual-stimuli. The surface morphologies, chemical compositions, charge, pH, and mechanical properties of these smart microgels were evaluated using scanning electron microscopy, IR, zeta potential measurements, pH evaluation, and quantitative nanomechanical mapping, respectively. Different oxidation states were observed when AP was introduced, as confirmed by UV spectroscopy and cyclic voltammetry. Systematic blood compatibility evaluations revealed that the SRHMGs have good blood compatibility. This bottom-up strategy to synthesize SRHMGs enables a new route to the production of smart microgels for biomedical applications.

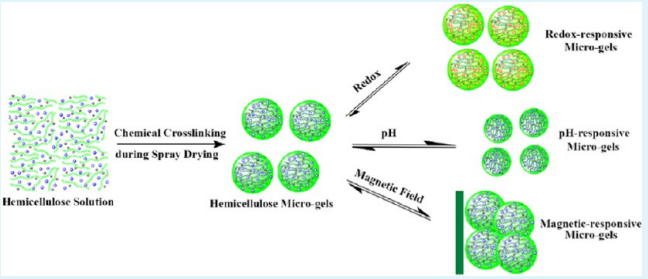

KEYWORDS: *cross-linking, microgel, hemicellulose, stimuli-responsive, spray drying, polysaccharides*

1. INTRODUCTION

Chemical cross-linking and curing have played vital roles in the alteration of the structure−property relationships of polymer materials. The highly cross-linked structure of a material is linked to superior mechanical properties, such as high modulus, high fracture strength, and solvent resistance. Conventional cross-linking chemistry includes polycondensation with multifunctional monomers leading to chain growth and simultaneous formation of a chemical network.[1] Recently, a broad range of cross-linking chemistries have been applied to create advanced materials that can perform self-healing mechanisms triggered by Diels−Alder couplings, photochemical reactions, disulfide bridges, radical fission, anionic reactions, or pH.[2] Unfortunately, some cross-linking processes create harsh environments that cause incompatibility with living cells and tissues if the material is utilized in biomedical applications.[3,4] Some processes are also time-consuming and/or include many steps to create a densely cross-linked structure in polymer-based materials.[5,6]

Hemicellulose, a byproduct in the wood industry, is categorized as the second most abundant group of polysaccharides in plants after cellulose and constitutes 15−35% (w/w) of wood and higher plants.[7] The existence of multiple hydroxyl groups on the hemicellulose backbone potentially creates a number of possibilities for chemical modification and preparation of materials with new profiles to enhance the utility of these natural polymers.[8] Hemicellulose hydrogels have been developed via robust cross-linking pathways, which is attributed to the excellent solubility of *O*-acetyl-galactoglucomannan (AcGGM) in water, dimethylformamide (DMF), and dimethyl sulfoxide (DMSO).[9] Multistep reactions and tedious purification are challenges necessary to overcome to produce other advanced materials from hemicellulose that cover a broad range of applications and that are tunable to the desired environment by oxidation−reduction (redox), pH, and electric and magnetic field stimuli.

Microgels are micrometer-sized cross-linked hydrogels, which have great potential for use in organic dye removal, controlled surface patterning, and vocal fold regeneration, as well as for use as drug delivery carriers and cell culture

Received: December 2, 2014
Accepted: January 29, 2015
Published: January 29, 2015

DOI: 10.1021/am5084732
ACS Appl. Mater. Interfaces 2015, 7, 4202−4215

Table 1. Parameters for Spray-Drying Process

name	aspirator degree (%)	inlet temperature (°C)	outlet temperature (°C)	gas flow (mL/min)	pump (%)
H_{40}	100	185 ± 3	85 ± 2	45	10
$H_{40}AP_{16}$	100	185 ± 2	85 ± 4	35	10
$H_{40}PAA_8$	100	185 ± 3	85 ± 3	45	10
$H_{40}Fe_{16}$	100	185 ± 2	85 ± 3	45	10
$H_{40}AP_8PAA_4$	100	200 ± 3	100 ± 4	45	10

substrates.[10−14] Microgels, such as bulk hydrogels, are three-dimensional hydrophilic networks that can absorb up to multiple times their dry weight in water and therefore enable mimicking of the extracellular environment of human organs.[15] The particular structure and low viscosity of microgel suspensions make it possible to inject them into the human body.[16] An attractive subclass of microgels is stimuli-responsive microgel, in which the volumetric expansion is a response to external stimuli such as pH, ionic strength, light, or temperature.[17−21] Dual stimuli-responsive microgels have recently been developed that respond to temperature and solvent concentration,[22] magnetic field and temperature,[23] pH and ionic strength,[24] pH and an applied electric field,[25] and temperature and UV light.[26] In addition, multiresponsive microgels have attracted much attention because their multifunctions can mimic the complex microenvironments in the human body[27−29] and potentially embrace a wide range of applications. They have also been created to respond to the combined stimuli of (1) the temperature, pH, and light irradiation,[27] (2) the temperature, pH, and magnetic field,[28] and (3) the ionic strength, temperature, and pH.[29]

Spray drying offers advantages such as efficiency, high yield, reproducibility, and more controllable distribution of particle size compared with other particle fabrication techniques.[30,31] Thus, the production of spray-dried microparticles has gained interest and is widely used in the pharmaceutical, food, and chemical industries.[32,33] Spray drying has been used to produce a reproducible coating layer of hemicellulose particles on polyethylene terephthalate substrates,[34] stereocomplexed particles of a poly(lactic acid) and poly(D-lactide) polymer blend,[35] and inorganic particles consisting of a mixed Ti/Al_2O_3 as a functional artificial tooth root.[36] It has also been used to modify calcium phosphate bone cement composites[37] and to fabricate antigen-loaded porous polyelectrolyte microparticles for use in oral antigen delivery.[33] If a strategy was developed for mediating the cross-linking of microgels during spray drying, it could be connecting the chemical modification of materials and industrial processing.

Our aim is to develop a facile, fast, and functional (3F) approach to creating stimuli-responsive hemicellulose microgels (SRHMGs) by single-step chemical cross-linking of AcGGM during spray drying. Using this strategy, cross-linking hemicellulose hydrogels with new profiles enhances their physicochemical properties in a broad range of applications. AcGGM was used to achieve renewable and value-added products; the poly(acrylic acid) (PAA), aniline pentamer (AP), and iron (Fe) additive provide SRHMGs that are responsive to external changes in pH, electrochemical stimuli, magnetic field, or a combination (dual-stimuli). We anticipate that this strategy will offer a 3F approach to produce SRHMGs without tedious purification because the solvent and the unreacted cross-linker will be removed during spray drying.

2. EXPERIMENTAL SECTION

2.1. Materials. Hydrochloric acid (HCl), sodium hydroxide (NaOH), disodium hydrogen phosphate (Na_2HPO_4), monosodium phosphate (NaH_2PO_4), epichlorohydrin (ECH), iron (Fe, 35−45 nm) particles, and PAA (35 wt % aqueous solution) were purchased from Sigma-Aldrich and used as received unless otherwise stated. Citric acid monohydrate ($C_6H_8O_7{\cdot}H_2O$) was obtained from Acros Organics. AcGGM originating from spruce (*Picea abies*) was extracted from thermomechanical pulping (TMP) processed water, purified, concentrated by ultrafiltration (membrane cutoff 1 kDa), and lyophilized using a Lyolab 300 lyophilizer. The carbohydrate composition of the AcGGM isolate was 17 mol % glucose, 65 mol % mannose, and 15 mol % galactose. AcGGM had a number-average molecular weight (M_n) of approximately 7500 g mol^{-1} (DP ≈ 40), a dispersity ($Đ$) of 1.3, and a degree of acetylation (DS_{Ac}) of 30%, as determined by size exclusion chromatography (SEC) calibrated with matrix-assisted laser desorption ionization time-of-flight mass spectrometry.[38] The AP was synthesized according to a previous report.[39]

2.2. Methods. *Fabricating Microgels.* The cross-linked hemicellulose-based microparticles were prepared in a one-pot approach. The mixture of 1200 mg of AcGGM, 1200 mg of NaOH, 1440 mg of ECH, and certain amount of functional materials were dissolved in 30 mL of water. The solutions were fed from the glass container, heated at 185−200 °C with a 35 m^3/min aspirator, and then sprayed out as fine droplets into the drying chamber, using a Mini Spray Dryer B-290 (Büchi Labortechnik AG, Switzerland). By means of an air flow (500−700 Nl/h), the droplets were transported into a small chamber and eventually precipitated into particles in a small vial. The prepared solutions were sprayed through the 0.7 mm fluid nozzles in the spray dryer. The detailed parameters for spray-drying procedure are listed in Table 1. The particles were washed with 50 mL of deionized water and centrifuged at 5000 rpm five times. The stimuli-responsive hemicellulose microgels were obtained after freeze-drying for 2 d and kept in the desiccator.

Scanning Electron Microscope. The morphology of the stimuli-responsive hemicellulose microgels was observed by Ultra-High Resolution FE-SEM (Hitachi S-4800). The samples were lyophilized overnight in small vials, attached to the sample supports using carbon tape, and coated with a 3.5 nm gold layer.

Fourier Transform Infrared. FTIR spectra were recorded using a PerkinElmer Spectrum 2000 spectrometer (PerkinElmer Instrument, Inc.) equipped with a single reflection attenuated total reflectance (ATR) accessory (golden gate) from Graseby Specac (Kent, U.K.). FTIR was used to verify the molecular structure of the stimuli-responsive hemicellulose microgels in a dry state. Each spectrum was recorded as the average of 16 scans at a resolution of 4 cm^{-1} between 4000 and 600 cm^{-1}.

Thermogravimetric Analysis. For the thermal stability of the hydrogels, thermogravimetric analysis (TGA) of the stimuli-responsive hemicellulose microgels was performed using a Mettler-Toledo TGA/SDTA 851e. Approximately 10 mg of each sample was put into a 70 μL ceramic cup without a lid. TGA tests were conducted under an N_2 atmosphere (flow rate of 50 mL/min) with a heating rate of 10 °C/min from 30 to 800 °C. The data were collected and analyzed with Mettler STARe software.

UV−vis Tests. The UV−vis spectra of $H_{40}AP_{16}$ and $H_{40}AP_8PAA_4$ microgels in pH 2.2−7.4 buffer solution were recorded on a UV−vis spectrophotometer (UV-2401) with a wavelength of 280−900 nm.

Cyclic Voltammetry. CV measurements of the $H_{40}AP_{16}$ and $H_{40}AP_8PAA_4$ microgels were performed on a potentiostat with a

DOI: 10.1021/am5084732
ACS Appl. Mater. Interfaces 2015, 7, 4202−4215

Table 2. Compositions of Cross-Linked Microgels

name	function	AcGGM (mg)	functional materials (mg)		NaOH (mg)	ECH (mg)	H_2O (mL)
H_{40}	No	1200		0	1200	1440	30
$H_{40}AP_{16}$	electroactivity	1200	AP	480	1200	1440	30
$H_{40}PAA_8$	pH response	1200	PAA	240	1200	1440	30
$H_{40}Fe_{16}$	magnetism	1200	Fe powder	480	1200	1440	30
$H_{40}AP_8PAA_4$	dual-function	1200	AP/PAA	240/120	1200	1440	30

scan rate of 60 mV·s^{-1}. Platinum wires were used as the working and auxiliary electrodes, and a K/KCl electrode was used as the reference. The samples were prepared by dispersing 15 mg of the $H_{40}AP_{16}$ and $H_{40}AP_8PAA_4$ microgels in 6 mL of DMSO and doping the sample with three drops of 2 M HCl.

Zeta Potential Measurements. Zeta potential measurements were performed on a Nano Zetasizer with a 633 nm He−Ne laser from Malvern Instrument U.K., Inc. Stimuli-responsive hemicellulose microgels (0.8 g/L) were prepared with pH 2.2−7.4 buffer solution: pH 2.2−6.38 buffer solutions were prepared from $C_6H_8O_7{\cdot}H_2O$, HCl, and NaOH; pH 7.4 buffer solution was prepared from Na_2HPO_4 and NaH_2PO_4. Each sample was measured three times, while each measurement consisted of 30 acquisitions. A 120 s delay between each measurement was used to prevent "charging" of the sample. All samples were measured at 25 °C with thermal conducting plates and 1 min of thermal equilibration.

Swelling Ratio Measurements. The swelling ratio (SR) of the hydrogels was determined by immersing dry hydrogels in buffer solutions (prepared from Na_2HPO_4 and NaH_2PO_4, pH = 7.4) at room temperature. The weights of the samples in the swollen state ($m_{s,t}$) at different time points were measured after gently removing excess water with filter paper. The SR was calculated using eq 1, where m_d denotes the weight of the samples in the dry state.

$$\mathrm{SR}(\%) = \frac{m_{s,t} - m_d}{m_d} \times 100 \tag{1}$$

Vibrating Sample Magnetometer. A vibrating sample magnetometer (EG&G Princeton Applied Research VSM model 155) was used to detect the room-temperature magnetic hysteresis loops. For each sample the data was collected at magnetic fields in the range of ±500 kA m^{-1} to determine the magnetization.

Atomic Force Microscopy. Mechanical properties on the hemicellulose-based microspheres surface were characterized using PeakForce Quantitative Nanomechanical Mapping (QNM) mode (PeakForce QNM) of a nanoscope V8 multimode AFM (Digital Instruments, Santa Barbara, CA) via 7850 EV scanner under ambient condition. The particulate samples were scanned using silicon-based cantilever (TAP150, P/N MPP-12120-10) with nominal spring constant of 5 N/m at a resonant frequency of 150 kHz. Actual spring constant of cantilever was in the range of 4.1−4.4 N/m after calibration with the thermal tune method. The calibrated cantilever was ramped three times on the selected areas of 200 nm × 200 nm on the hard surface (silica) to get the updated sensitivity. It was later scanned on a standard polystyrene/low density polyethylene (PS/LDPE) sample that was already known its mechanical contact. During nanomechanical measurements, the obtained force profiles were analyzed using Derjaguin−Muller−Toporov model.[40]

According to this model, mechanical contact was expressed from the following equation.

$$a = \sqrt[3]{\frac{R}{E_{tot}}(F + 2\pi RW)} \tag{2}$$

$$\delta = \frac{a^2}{R} = \frac{(F + 2\pi RW)^{2/3}}{\sqrt[3]{RE_{tot}^2}} \tag{3}$$

where a, δ, F, R, W, and E_{tot} are tip−sample contact radius, deformation, adhesion force, tip radius, work of adhesion per unit area, and the reduced Young's modulus, respectively.

Clotting Time. To evaluate the antithrombogenicity of the stimuli-responsive hemicellulose microgels, activated partial thromboplastin time (APTT) and thrombin time (TT) were measured by an automated blood coagulation analyzer CA-50 (Sysmex Corporation, Kobe, Japan) according to the method described in a previous report.[41] Healthy human fresh blood was collected in vacuum tubes containing sodium citrate as the anticoagulant (anticoagulant to blood ratio, 1:9 v/v), and the platelet-poor plasma (PPP) was obtained after centrifuging at 4000 rpm for 15 min. Stimuli-responsive hemicellulose microgels (10 mg/mL) were prepared in buffer solution (pH = 7.4), 5 μL suspensions and 100 μL of PPP were incubated at 37 °C for 0.5 h, and 50 μL of incubated solution was then added to the test cup, followed by the addition of 50 μL of APTT agent (Dade Actin Activated Cephaloplastin Reagent, Siemens; incubated 10 min before use). The solution was incubated at 37 °C for another 3 min, and 50 μL of 0.025 M $CaCl_2$ was subsequently added. The APPT was recorded by an automated blood coagulation analyzer CA-50. Two independent measurements were averaged to reach a reliable value. The TT test was performed in a process similar to that of the APTT test. The only difference is the APTT agent replaced by Test Thrombin Reagent (Siemens; incubated 10 min before use).

Hemolysis Test. The hemolysis test was performed as previously reported.[42] In brief, 10 mL of whole blood was added to 20 mL of phosphate-buffered saline (PBS) solution (pH = 7.4) and then centrifuged at 500 g for 10 min five times to isolate red blood cells (RBCs) from human plasma, and the RBCs were diluted into PBS solution with a final volume of 100 mL. Then, 0.2 mL of the diluted RBC suspension (~5 × 10^8 cells/mL) was added to 1.8 mL of the 20 mg/mL stimuli-responsive hemicellulose microgels. Deionized water dispersed RBCs was used as the positive control, and the PBS (pH 7.4) dispersed RBCs were used as the negative control. All the suspensions were incubated in a rocking shaker at 37 °C for 3 h and then centrifuged at 10 016 g for 3 min. The absorbance of the released hemoglobin in the suspensions was measured at 540 nm using a UV−vis spectrophotometer. The hemolysis ratio was calculated using eq 4.

$$\text{hemolysis ratio}(\%) = \frac{\text{suspension}_{Abs} - \text{negativecontrol}_{Abs}}{\text{positivecontrol}_{Abs} - \text{negativecontrol}_{Abs}} \tag{4}$$

Whole Blood Clotting Time. To investigate the whole blood clotting time (WBCT), 10 μL of the 10 mg/mL microgels suspension in pH 7.4 buffer solution was added to 50 μL of fresh blood without any anticoagulant, and timing was begun immediately just after the blood came in contact with the particles. The whole blood was monitored for clotting by manual dipping with a stainless-steel wire hook coated with silicone into the blood to detect fibrin threads. The clotting time was recorded at the first sign of any fibrin formation on the hook. The test was repeated three times for each sample, and a reliable value was obtained.

3. RESULTS AND DISCUSSION

In the past decade, spray drying has been used to produce coatings[34] and microparticles[35] due to its efficiency, high yield, and reproducibility. Here, a chemical cross-linking process during spray drying was developed to produce hemicellulose microgels to achieve value-added and renewable products. The combination of the biocompatibility of hemicellulose and the

DOI: 10.1021/am5084732
ACS Appl. Mater. Interfaces 2015, 7, 4202−4215

Scheme 1. SRHMG Production (with $H_{40}AP_{16}$ as an example) via a Spray Dryer

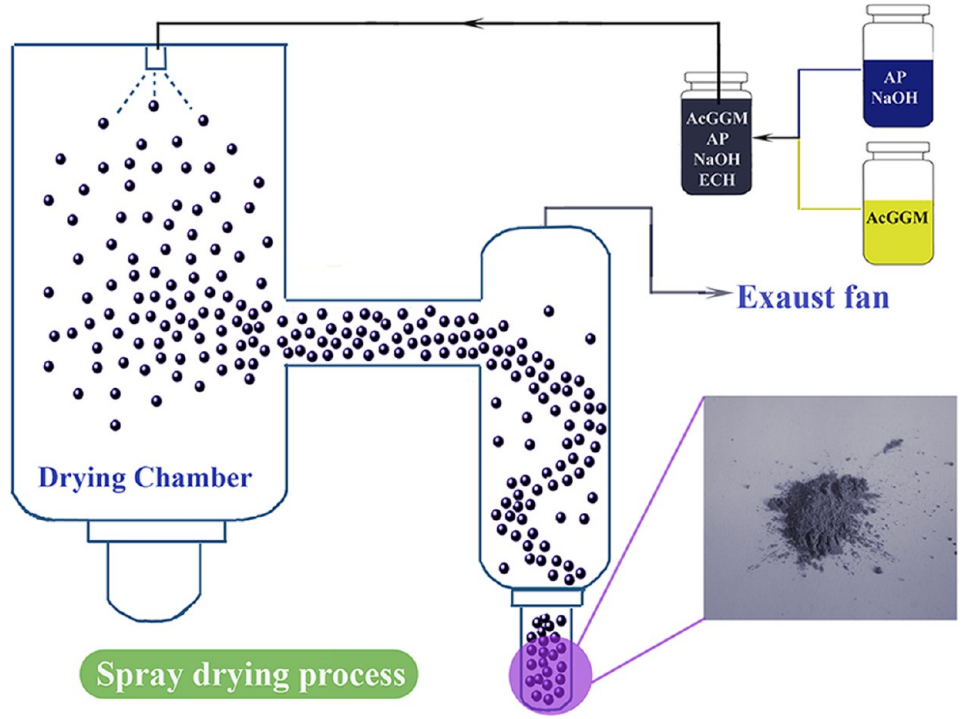

promising properties of the functional additives may offer possibilities for the use of SRHMGs in biomedical applications.

3.1. Microgel Synthesis. The SRHMGs were prepared via a 3F spray-drying process. A mixture of 1200 mg of AcGGM, 1200 mg of NaOH, 1440 mg of ECH, and specific amounts of functional materials were dissolved in 30 mL of water. The solutions were pumped and heated to 185−200 °C at the nozzle and then sprayed out as fine droplets into a glass chamber using a mini spray dryer (B-290, Büchi Labortechnik AG, Switzerland). PAA, AP, and Fe nanopowders were chosen as stimuli-responsive additives to offer pH sensitivity, electroactivity, and magnetic response, respectively. The compositions of the reaction mixtures for the cross-linked microgels are shown in Table 2. The SRHMGs were annotated according to their concentrations (% w/v) in water. For example, $H_{40}AP_{16}$ contained 40 g/L of AcGGM and 16 g/L of AP in an aqueous solution. Microgels without functional additives (H_{40}) were synthesized as reference samples and were denoted according to the same system.

The developed spray-drying process is shown in Scheme 1 with the sample $H_{40}AP_{16}$ as an example. In addition to solubilizing AP, NaOH (aq) acted as a catalyst and a proton scavenger for the cross-linking reaction. A 40 g/L AcGGM aqueous solution could be cross-linked via 44 g/L ECH at room temperature in 12 h, or it could be cross-liked in 1 h when heated to 65 °C. Therefore, the hemicellulose network could be formed more rapidly when higher temperatures (185−200 °C) were used during the spray-drying process, and the functional additives were eventually immobilized in the hemicellulose network. The short exposure time to the high outlet temperature minimizes the risk of thermal degradation of the hemicellulose polysaccharide backbone. The prepared SRHMGs combined the nontoxicity, biocompatibility, biodegradability, and renewability of AcGGM with the functionalities of PAA, AP, and Fe. The crude SRHMGs were dispersed in 35 mL of deionized water and centrifuged at 5000 rpm. Images of the microgels before and after centrifugation are shown in Figure S1 (Supporting Information). The SRHMGs were insoluble in water and remained at the bottom of the tubes after centrifugation, indicating that the cross-linking reaction was successfully performed and that no soluble fraction remained after spray drying.

There are several benefits of the present strategy: (1) a single-step cross-linking reaction occurs in situ during the spray-drying process; (2) the spray dryer operating conditions are easily tuned within a wide range to control the product quality; (3) compared with other routes, spray drying rapidly produces the desired gels (within a few minutes); and (4) because of the high processing temperature (200 °C), both the solvent (water, bp 100 °C) and the unreacted cross-linker (ECH, bp 114 °C) can be completely removed during spray drying.

Of the freshly prepared SRHMGs, the H_{40} (a-1) and $H_{40}PAA_8$ (c-1) microgels were lighter in color, whereas the $H_{40}AP_{16}$ (b-1) and $H_{40}Fe_{16}$ (d-1) microgels were darker due to the colored AP and Fe. SEM images of the SRHMGs are shown in Figure 1 (a-2, b-2, c-2, d-2, and e-2). Most of the microgels showed spherical morphologies, although a few of them had imperfect spherical or slightly shriveled structures depending on the functional additives that were cosprayed with the hemicellulose bulk material. The composition of the solution appeared to influence the morphology of the particulate materials. The microgel particle size distributions were calculated from the SEM analyses, also shown in Figure 1 (a-3, b-3, c-3, d-3, and e-3). The average particle size of the pure hemicellulose microgels (H_{40}) was ~2.0 ± 1.0 μm, whereas the $H_{40}AP_{16}$ and $H_{40}PAA_8$ microgels had the lowest average size (~1.3 ± 0.3 μm). The particle size increased to 2.7 ± 2.2 μm when AP and PAA were simultaneously added. Specifically, a narrow particle size distribution was observed when aniline oligomers (Figure 1b-3) or PAA (Figure 1c-3) was incorporated into and/or adsorbed onto the cross-linked

DOI: 10.1021/am5084732
ACS Appl. Mater. Interfaces 2015, 7, 4202−4215

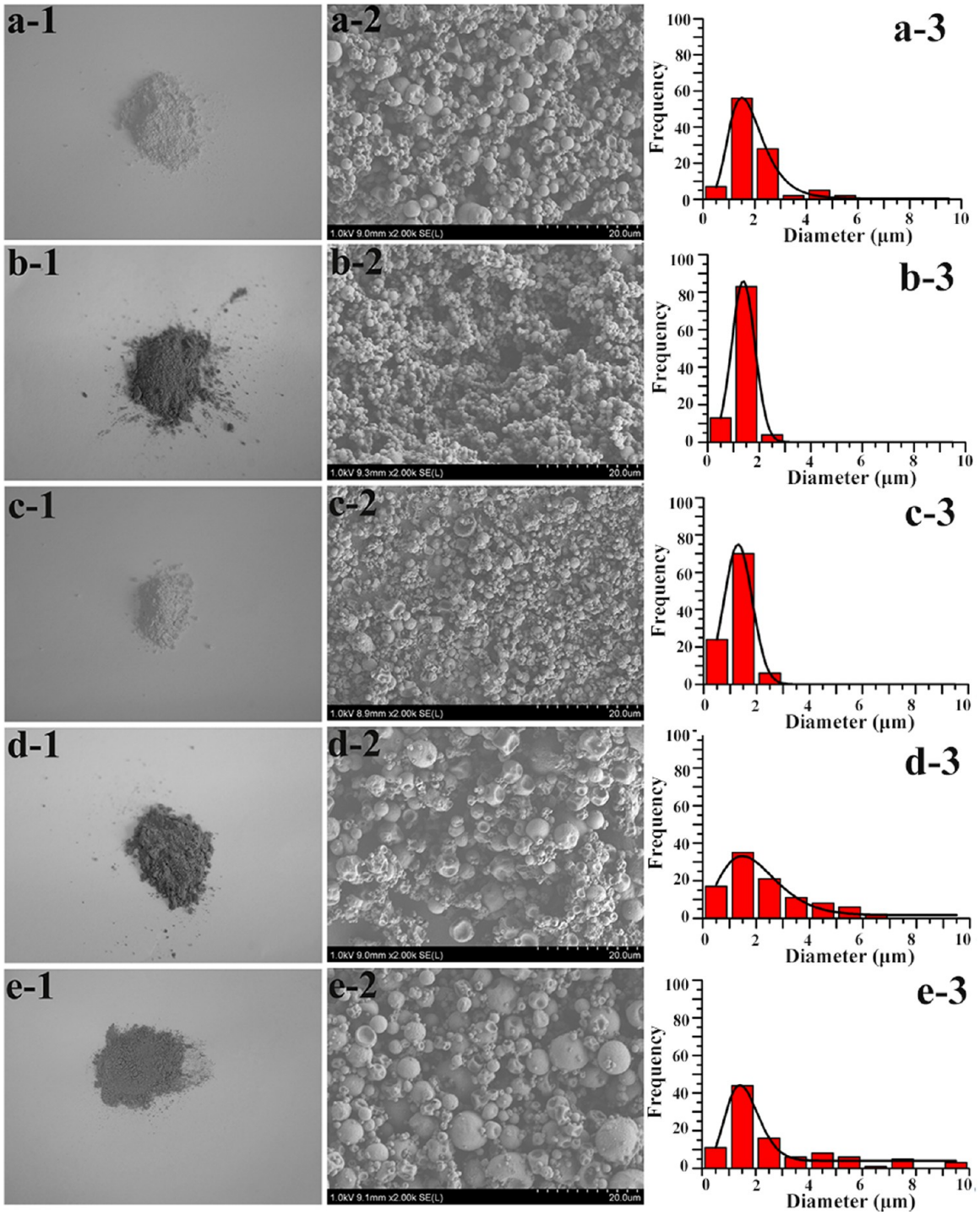

Figure 1. Freshly prepared SRHMGs (a-1, b-1, c-1, d-1, and e-1), SEM images (a-2, b-2, c-2, d-2, and e-2) and size distribution (a-3, b-3, c-3, d-3, and e-3) of H_{40} (a-1, a-2, and a-3), $H_{40}AP_{16}$ (b-1, b-2, and b-3), $H_{40}PAA_8$ (c-1, c-2, and c-3), $H_{40}Fe_{16}$ (d-1, d-2, and d-3), and $H_{40}AP_8PAA_4$ (e-1, e-2, and e-3).

hemicellulose. In contrast with the $H_{40}AP_{16}$ and $H_{40}PAA_8$ microgels, the introduction of AP and PAA resulted in the broadest particle size distribution (Figure 1e-3). Clearly, the particle size differed between compositions due to the introduction of additives. The diameter of the dried particle is dependent on its droplet size and density of the droplet and particle. The droplet itself is a function of the surface tension. A decrease in the microgel diameter is caused by strong surface tension. AP appeared to provide stronger attractive intermolecular interactions in the cross-linked hemicellulose network than PAA, resulting in strong surface tension. A smaller dried particle size could be then obtained. On the contrary, the introduction of AP and PAA simultaneously reduced the surface tension of the liquid droplet, leading to larger diameter particles due to stronger repulsive intermolecular interactions inside the hemicellulose matrix. Fe nanopowders have a high density and are insoluble in water (were in suspension in the present research), which induces a wide size distribution of

DOI: 10.1021/am5084732
ACS Appl. Mater. Interfaces 2015, 7, 4202−4215

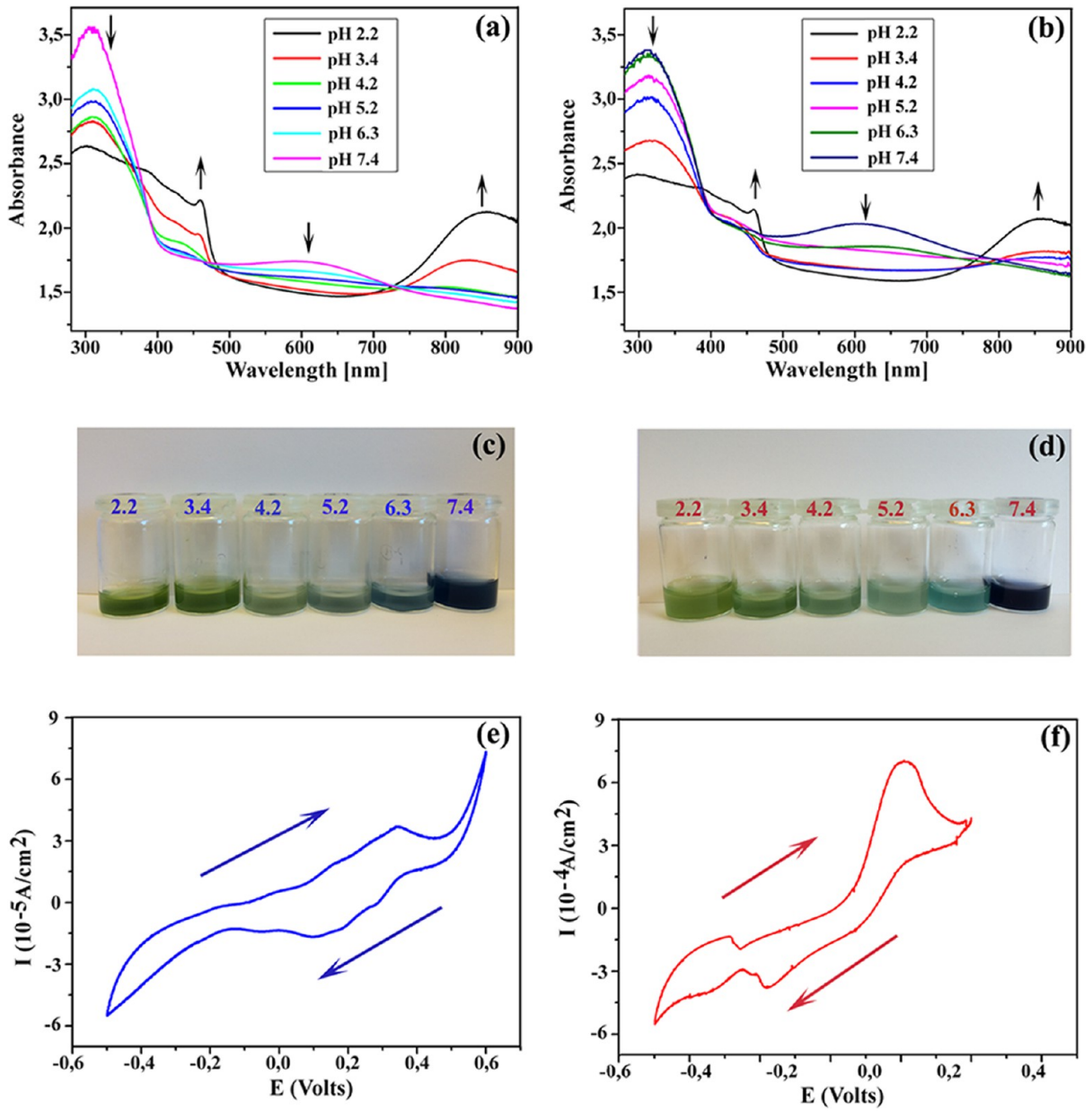

Figure 2. UV−vis spectra of $H_{40}AP_{16}$ (a) and $H_{40}AP_8PAA_4$ (b) in different pH aqueous buffer solutions. Images of $H_{40}AP_{16}$ (c) and $H_{40}AP_8PAA_4$ (d) in different pH aqueous buffer solutions. Cyclic voltammograms of $H_{40}AP_{16}$ (e) and $H_{40}AP_8PAA_4$ (f) in DMSO doped with three drops of 2 M HCl solution.

$H_{40}Fe_{16}$ microgel particles. The $H_{40}Fe_{16}$ microgels had an average size greater than 1 μm, and magnetic field responsive particles in this size range can be used for bowel contrast (mean diameter no less than 300 nm) and liver/spleen imaging.[43] In addition, the dispersibility of the cross-linked microgels was assessed to calculate their hydrodynamic diameters using dynamic light scattering. The retrieved data was, however, ambiguous due to the somewhat irregular shape, wide size distribution, and polydispersity of the cross-linked microgels. As an alternative, we used an SEM coupled with energy-dispersive spectrum (EDS) analysis to evaluate not only the size and structural information on the cross-linked microgels (Figure 1) but also the existence of functional additives such as Fe that were randomly distributed on the surface (Figure 5B).

The IR spectra of the SRHMGs are shown in Figure S2 (Supporting Information). The pristine hemicellulose microgels displayed an H−O−H deformation vibration of absorbed water at ∼1635 cm^{-1} and a hydroxyl band at 3000−3600 cm^{-1} (Figure S2a). The C═O stretching at 1730 cm^{-1} stemming from the acetylated pendant groups disappeared due to the deacetylation of AcGGM in the presence of NaOH.[44] The IR spectrum of $H_{40}AP_{16}$ in Figure S2b shows not only amide group absorption at 1655 cm^{-1} and the characteristic peaks of the benzenoid ring at 1601 and 1509 cm^{-1} from AP but also the signals from the H_{40} microgel, indicating that AP was incorporated into and/or adsorbed onto the hemicellulose-based microgels. In contrast, the $H_{40}PAA_8$ microgel spectrum showed −C−O− group absorption bands at 1662 and 1570 cm^{-1} from PAA (Figure S2c). The ATR-FTIR spectrum of the $H_{40}AP_8PAA_4$ microgel in Figure S2e shows the signals of both $H_{40}AP_{16}$ and $H_{40}PAA_8$, which indicated the successful introduction of PAA and AP into the composite microgels.

DOI: 10.1021/am5084732
ACS Appl. Mater. Interfaces 2015, 7, 4202−4215

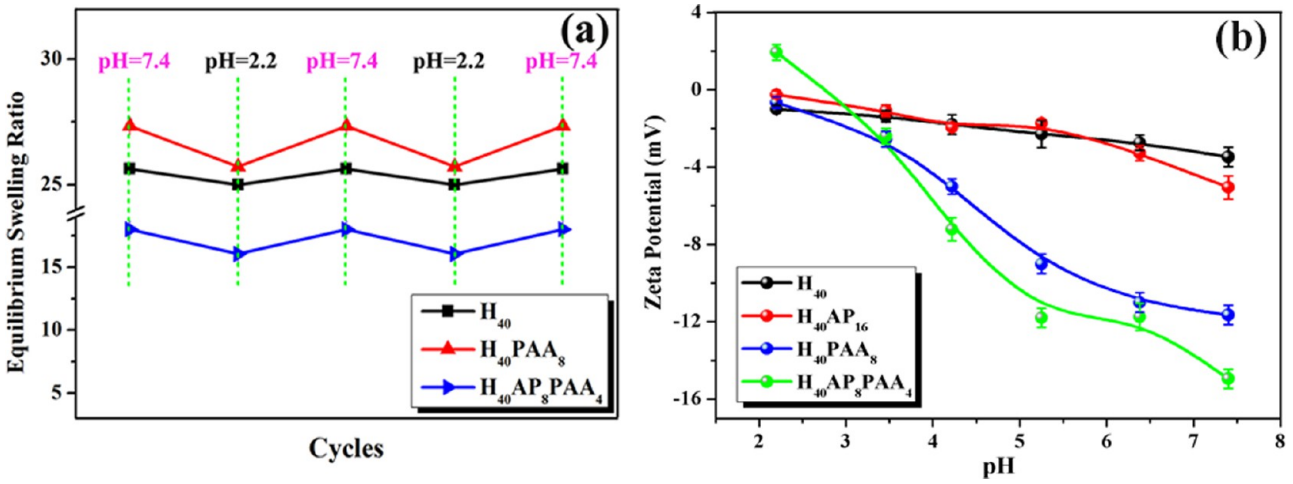

Figure 3. Equilibrium swelling ratio of the SRHMGs under repeated pH changes between 7.4 and 2.2 (a). Zeta potential of the SRHMGs (b).

Compared with H_{40}, all of the other microgels displayed a small peak at 1736 cm^{-1}, which was attributed to acetylated pendant groups that indicated that the deacetylation of AcGGM was not complete.

Because the thermal decomposition of AcGGM and the functional additives are different, the thermal behavior of the SRHMGs yields information about the microgel composition (Figure S3 in the Supporting Information). The hemicellulose hydrogel (H_{40}) underwent degradation between 300 and 400 °C. At temperatures above 400 °C, all of the functional microgels had lower weight loss compared with the pure hemicellulose microgel (H_{40}) due to the higher onset temperatures for thermal degradation of the functional additives. For the $H_{40}Fe_{16}$ microgel, a sharp decrease in weight (or force) at 575 °C was due to the Curie temperature (loss of ferromagnetism) of the magnetic particles.[45]

The images, the IR spectra, and the thermal decomposition of the SRHMGs convinced us that the stimuli-responsive additives were blended with the hemicellulose-based microgels. The content and percent incorporation efficiency of functional additives in the SRHMGs are shown in Supporting Information, Table S1. The percent incorporation efficiencies of various stimuli-responsive additives are 70, 84, 42, and 52% for $H_{40}AP_{16}$, $H_{40}PAA_8$, $H_{40}Fe_{16}$, and $H_{40}AP_8PAA_4$ microgels, respectively.

3.2. Electroactivity of the Microgels. The ability of materials to transmit bioelectrical signals in vivo and/or in vitro plays a significant role in their applications in the biomedical field. To make a polymeric material electroactive, the electrons must move within the materials, which is enabled by oxidation or reduction.[46] AP is made electroactive via chemical or electrochemical oxidation or reduction, which is attributed to its conjugated structure. By introducing AP, hemicellulose microgels are able to exhibit electroactivity. The minimum pH in the human body is ~1−2 in the stomach, whereas the body pH level (blood) is slightly alkaline (pH ≈ 7.4). Therefore, the UV−vis spectra of 0.8 g/L $H_{40}AP_{16}$ (a) and $H_{40}AP_8PAA_4$ (b) microgels were recorded in buffer solutions in a pH range of 2.2−7.4 (Figure 2). The $H_{40}AP_{16}$ (a) and $H_{40}AP_8PAA_4$ (b) microgel suspensions showed two characteristic peaks at 310 and 609 nm corresponding to the benzene and quinoid groups at pH 7.4, respectively. Interestingly, these two peaks gradually decreased with decreasing pH. The peak at 609 nm almost disappeared when the pH of the aqueous buffer solution reached 2.2. Two new peaks at 461 and 850 nm were related to the formation of polarons from the electron transition of quinoid to benzenoid units, as shown in Figure S4 (Supporting Information).[47] The intensities of these two peaks increased with decreasing pH. The more H^+ ions in solution, the higher the concentration of radical cations (polarons) formed. In other words, the reaction shifted to the polaron direction as the pH decreased. This result explains why the color of the $H_{40}AP_{16}$ (c) and $H_{40}AP_8PAA_4$ (d) microgel solutions altered with pH (Figure 2).

AP exhibits four different oxidation states of the aniline segments: the fully reduced leucoemeraldine (LMAP), the emeraldine I (EMAP I), the emeraldine II (EMAP II), and the fully oxidized pernigraniline state.[46,48] The $H_{40}AP_{16}$ and $H_{40}AP_8PAA_4$ microgels were prepared with the fully reduced LMAP or the partially oxidized EMAP. Cyclic voltammetry (CV) of $H_{40}AP_{16}$ (e) and $H_{40}AP_8PAA_4$ (f) in DMSO doped with three drops of 2 M HCl solution confirmed that the microgels were electroactive and that the AP in these microgels retained its ability to be repeatedly oxidized and reduced. The CV measurements also confirmed the reversibility of oxidation and reduction. The $H_{40}AP_{16}$ microgels (e) exhibited three characteristic redox peaks for AP (Figure S5 in the Supporting Information). The first redox peak corresponded to the transition from the LMAP state to the EMAP I state, the second one from the EMAP I state to the EMAP II state, and the last one from the EMAP II state to the fully oxidized pernigraniline state (Figure S6, Supporting Information).[46,48] However, the second redox peak for the $H_{40}AP_8PAA_4$ (f) microgel almost disappeared. The reason for this result might be due to the complex interaction between AP and the polymeric dopant PAA that allows AP to be quickly oxidized and reduced from the EMAP I state to the EMAP II state.

3.3. Microgel pH Sensitivity. The swelling behavior of the microgels was assessed in the 2.2−7.4 pH range to demonstrate the pH sensitivity of the hybrid microgels (Figure 3). The equilibrium swelling ratio of the pure hemicellulose (H_{40}) microgels was as high as 25.5 at pH = 7.4, which was due to the hydrophilicity of AcGGM. This value for the H_{40} microgels was stable even after two cycles of acidic/alkine treatments. The $H_{40}PAA_8$ microgels exhibited a swelling/deswelling behavior as the solvent conditions changed from pH = 7.4 to pH = 2.2. Interestingly, the $H_{40}PAA_8$ microgels had a higher equilibrium swelling ratio in comparison with that of the H_{40} microgels,

DOI: 10.1021/am5084732
ACS Appl. Mater. Interfaces 2015, 7, 4202−4215

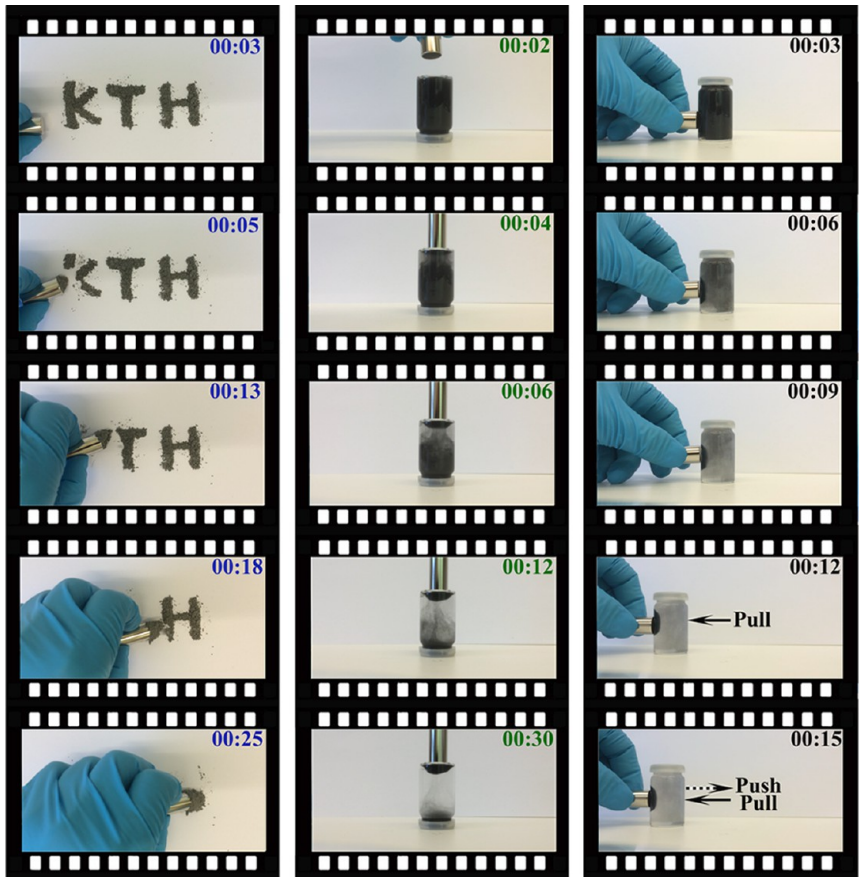

Figure 4. Photos of SRHMGs ($H_{40}Fe_{16}$) in a magnetic field: solid powder state (left); 10 mg/mL in water with a magnet field supplied at the bottom of the vial (middle); 10 mg/mL in water with a magnet field supplied at left side of the vial (right).

which was likely due to the hydrogen bonding between the hemicellulose (AcGGM) and PAA. PAA is a weak polyacid that is sensitive to pH. At low pH, the acrylic acid groups undergo protonation, and they become more ionized with increasing pH. In other words, repulsive interactions among neighboring PAA chains tend to provide a strong swelling effect, in particular at high pH, as shown in Figure 3a. Thus, their swelling behavior is governed by conformational changes of the polymeric chains from low to high pH values. The equilibrium swelling ratio of the $H_{40}AP_8PAA_4$ microgels decreased due to the addition of AP.[44] This result might be due to attractive interactions between the acrylic acid groups and AP, shrinking the chain conformation and shifting to deswelling behavior. The pH reversibility of the swelling ratios of the $H_{40}PAA_8$ and $H_{40}AP_8PAA_4$ microgels is also an indirect way to confirm the successful cross-linking of hemicellulose. The resulting microgels can swell and deswell in a predictable way as the solvent conditions change based on environmental stimuli (pH), thereby enabling improved control over their properties relative to other reported approaches.

The flexibility in tuning the charge properties of the microgels makes them a suitable choice for various biological applications.[49] Zeta potential measurements demonstrate whether the microgels have a positive or negative surface charge. It can also be used to evaluate the microgel stability in a liquid at specific pH values. The higher the zeta potential, the higher the stability of the particle suspension.[50] The zeta potentials of the SRHMGs reflected their charge properties. They were recorded on a Nano Zetasizer and plotted in Figure 3b. The zeta potential of all of the microgels decreased as the pH increased. The H_{40} microgels had an almost linear relationship between the zeta potential and pH. The $H_{40}AP_{16}$ microgels showed a decrease in zeta potential compared with the H_{40} microgels at pH > 6 because of the ability of AP to move protons. The $H_{40}PAA_8$ microgels had a significant zeta potential decrease at pH > 4 continuing to −11 mV due to the pK_a of PAA (~4.1). The carboxyl group of PAA is deprotonated when the pH is greater than the pK_a of PAA, and both the bulk and surface of the microgels are therefore negatively charged, resulting in a dramatic decrease in the zeta potential to more negative values. The difference between H_{40} and $H_{40}PAA_8$ is that the latter contain PAA, which effectively is a polyelectrolyte with ionizable pendant groups in every repeating unit. Hence, $H_{40}PAA_8$ is sensitive toward changes in pH, which will be reflected in a significant change in the surface charge of the microgels. When AP was added to the microgels (H_{40}), the starting zeta potential was ~2 mV, which was followed by a sharp decrease, finally reaching a value of −15 mV. The reason for this result was because PAA could be a polymeric dopant of AP, and they created a synergistic effect on their zeta potentials. The $H_{40}AP_8PAA_4$ microgels were the most stable of the microgels at high pH due to more negative zeta potential. This result means that their tendency to aggregate in liquid is much less compared with other microgel-based systems. All of the SRHMGs had a lower zeta potential at pH 7.4 than the pure hemicellulose microgels, indicating their possibility for use in biomedical applications.

DOI: 10.1021/am5084732
ACS Appl. Mater. Interfaces 2015, 7, 4202−4215

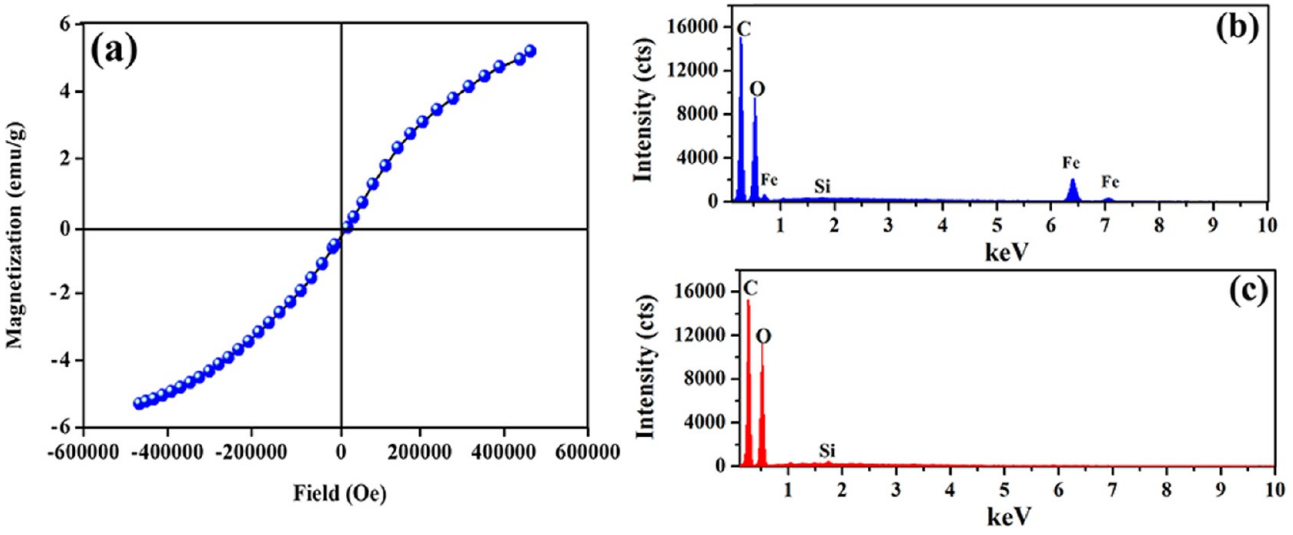

Figure 5. Magnetic hysteresis of $H_{40}Fe_{16}$ (a), EDS spectrum of $H_{40}Fe_{16}$ (b), and EDS spectrum of H_{40} (c) microgels.

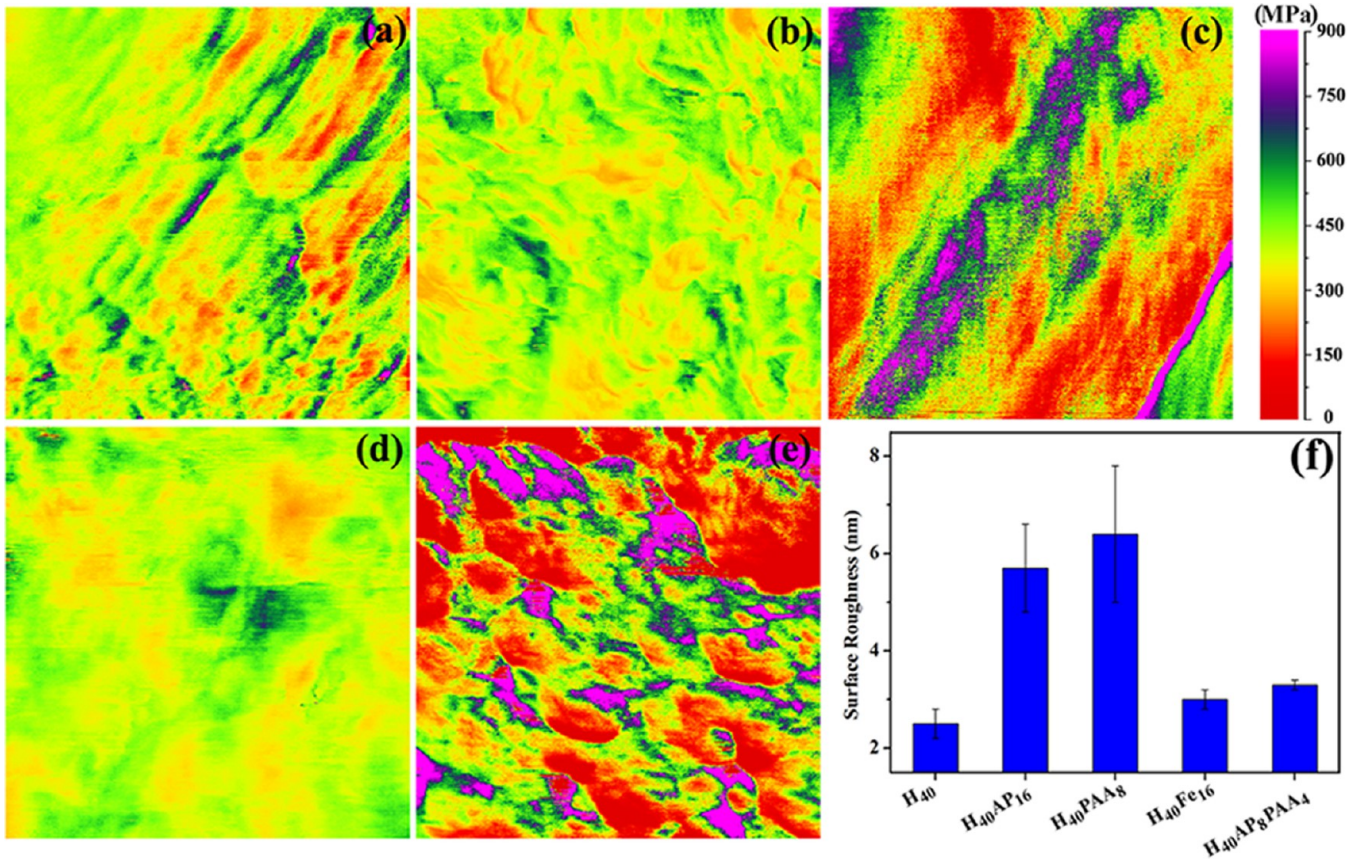

Figure 6. Young's moduli of the SRHMGs measured using QNM: H_{40} (a), $H_{40}AP_{16}$ (b), $H_{40}PAA_8$ (c), $H_{40}Fe_{16}$ (d), and $H_{40}AP_8PAA_4$ (e). (f) The surface roughness of these microgels.

3.4. Microgel Magnetic Response. Pictures of magnetic-responsive hemicellulose microgels ($H_{40}Fe_{16}$) placed in a magnetic field are shown in Figure 4. Clearly, the magnetic field-responsive hemicellulose microgels in the solid state could be adsorbed to magnets within 25 s (Figure 4, left) as a result of the presence of Fe nanopowders. Interestingly, the $H_{40}Fe_{16}$ microgels can be suspended into a 10 mg/mL aqueous solution (Figure 4, middle) due to the hydrophilicity of hemicellulose (AcGGM). These microgels assembled within 30 s at the bottom of the 10 mL vial where the magnetic field was applied. The magnetic field-responsive hemicellulose microgels could move directly to the left side of the vial in 10 s, and the vial could be pulled away due to the force between the magnetic field and the Fe nanopowders. Clearly, the magnetic field-responsive hemicellulose microgels possessed a magnetic response, which provides possibilities for use in biomedical applications. Magnetic field-induced transference is very important for drug controlled release, as well as in clinical

DOI: 10.1021/am5084732
ACS Appl. Mater. Interfaces 2015, 7, 4202−4215

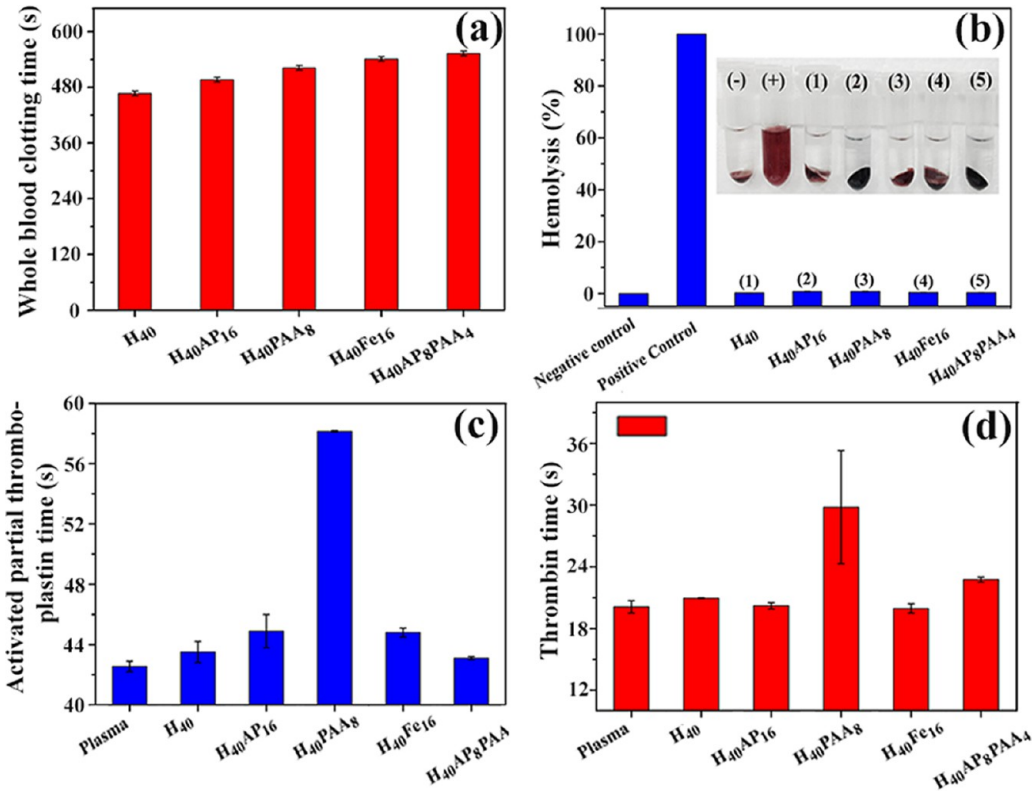

Figure 7. Blood compatibility measurements for the SRHMGs: (a) whole blood clotting time, (b) hemolysis, (c) activated partial thromboplastin time, and (d) thrombin time. Values are expressed as the mean ± standard deviation for $n = 3$.

diagnosis.[51] These microgels could hypothetically be loaded with drug and then delivered to specific locations. The videos related to Figure 4 are shown in the Supporting Information (Videos S1, S2, and S3).

The magnetization of the $H_{40}Fe_{16}$ microgels as a function of the magnetic field at 298 K was measured using a vibrating sample magnetometer , shown in Figure 5a. The magnetization of the $H_{40}Fe_{16}$ microgels increased with an increase in the magnetic field, indicating the successful synthesis of magnetic field-responsive hemicellulose microgels. To obtain the composition of the $H_{40}Fe_{16}$ microgels, the EDS from SEM was measured and is shown in Figure 5b. There was only C, O, and Fe in the composite microgels, whereas the microgels without Fe (H_{40}) only showed C and O (Figure 5c). The content of Fe in the $H_{40}Fe_{16}$ microgels was 6.8 (% w/w).

3.5. Microgel Mechanical Properties. Mechanical properties are often essential for microgels. In the pharmaceutical field, compact tablets prepared from compressed microparticles should have sufficient mechanical strength to withstand the various handling operations in the storage logistic chain to the patient.[52] In the tissue engineering field, some critical factors such as biocompatibility and a load bearing ability cannot be neglected when repairing damaged tissues. During tissue regeneration, the living cells can sense or detect the presence the mechanical properties in their surrounding environment and then convert these mechanical responses to chemical responses.[53] Quantitative nanomechanical mapping (QNM) was used to measure the stiffness of the cross-linked microgels, quantified as the effective Young's modulus of the microgels and determined by fitting the measured tip−surface contact force to the Derjaguin−Muller−Toporov model.[40,54,55] The adhesive forces between the substrate and the tip determine the Young's moduli. Compared with the mechanical properties of the H_{40} microgels (Figure 6a), the addition of AP and Fe into the hemicellulose matrix seemed to provide a narrow range distribution of the Young's moduli (Figure 6b,d). The high molar mass PAA varied the force between the substrate and the silicon-based tip (Figure 6c,e). When indenting soft polymers such as PAA, plastic deformation might occur, which means that the loading−unloading forces on the substrate surface do not overlap. The exerted force of the substrate surface varied from one position to another due to plastic deformation. An uneven mapping or a broader range distribution of the Young's moduli could be observed because they were determined by the interacting forces between the tip and the substrate surface. In contrast with the tip-PAA interaction, the introduction of small additives, namely, Fe and AP, might result in overlapping approach−withdrawal forces, leading to elastic deformation on the surface of the microgels. In other words, low molar mass additives such as Fe and AP gave rise to elastic deformation. From the mechanical mapping distribution, the cross-linked hemicellulose microgels demonstrated promising potential for use in a broad range of applications that demand strong mechanical properties on the surface. Different functional groups added to the hemicellulose microgels influenced the surface roughness. A segmental distribution of conformational chains, that is, loops, trains, or tails of the soft polymer (PAA), might affect the topography of the hemicellulose-based microgels, leading to an increase in the surface roughness. When AP was mixed with PAA, a flattened conformation might form during the microgel fabrication; therefore, a decrease in surface roughness was observed. A uniform distribution of Fe nanoparticles on the surface of the

DOI: 10.1021/am5084732
ACS Appl. Mater. Interfaces 2015, 7, 4202−4215

Scheme 2. Synthesis of SRHMGs and Suggested Application Fields of These Microgels

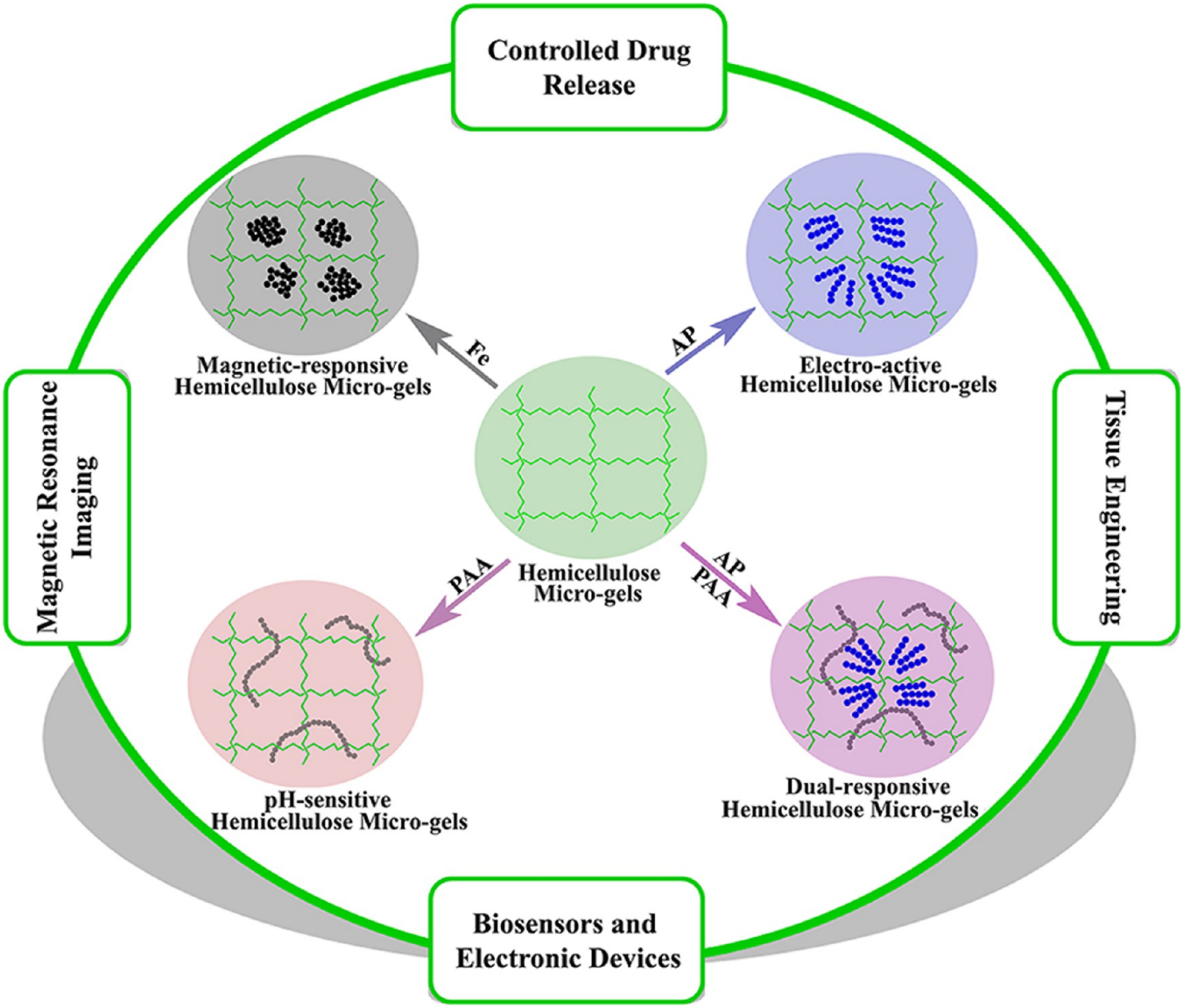

microgels slightly increased the surface roughness of the hemicellulose microgels (Figure 6f).

3.6. Microgel Blood Compatibility. Blood compatibility testing of the SRHMGs was performed via a systematic protocol and included measurements of the WBCT, APTT, and TT, as well as hemolysis testing. The WBCT measurement provides an overview of all of the intrinsic clotting factors in the absence of tissue factors, and it plays an important role in blood-compatible materials that are in direct contact with fresh blood.[56] Whole blood (50 μL) without any anticoagulant was used in the present test, and the results are shown in Figure 7a. The WBCT of the pure hemicellulose microgels (467 s) was much higher than that of poly(ether sulfone) (~88 s), the latter being a commonly used blood-contacting biomaterial.[51] All of the SRHMGs showed prolonged WBCTs with a maximum of 553 s.

The hemolysis test is to determine the solubility of the RBCs in contact with foreign materials and has been a powerful in vitro assay to evaluate the hemolysis property of biomaterials.[57] Hemoglobin is subsequently delivered from RBCs when the foreign material breaks the cells, and the hemolysis of foreign materials is then measured via the absorbance of visible light (Figure 7b). In general, a hemolysis percentage less than 5% is required for biomaterials to be used as drug release carriers or implanted devices. Both the pure hemicellulose microgels and SRHMGs had hemolysis percentages less than 3%, indicating that the hemicellulose has good blood compatibility, and the hemolysis effect of these SRHMGs is thus greatly suppressed.

The blood compatibility of the SRHMGs should be measured in depth (lower than cell level) to address the complicated microenvironment of the blood. Thus, APTT and TT were performed to address this need. The APTT test is a global screening procedure to evaluate coagulation abnormalities in the intrinsic pathway and the common plasma coagulation pathways including Factors II, V, X, or fibrinogen.[56,58] The TT test evaluates the clot formation time for thrombin to convert fibrinogen into fibrin in PPP.[41] The APTT (Figure 7c) and TT (Figure 7d) tests of the SRHMGs were performed in a 10 μg/mL solution. Both the pure hemicellulose microgels and SRHMGs showed APTT or TT values comparative with the control reference (plasma in this case). The $H_{40}PAA_8$ microgels had a clearly increased APTT

DOI: 10.1021/am5084732
ACS Appl. Mater. Interfaces 2015, 7, 4202−4215

(to 58 s) compared with the plasma, which was due to the presence of carboxyl groups on PAA. The TT of the $H_{40}PAA_8$ microgels exhibited the same behavior with a value of 30 s. The prolonged APTT for the surface-immobilized carboxyl groups has no relationship with the deficiency of Factor XII (likely related to other components in plasma, such as calcium ions).[59] The interactions between carboxyl groups and calcium ions prevent the formation of thrombin clots, and further led to prolonged clotting times (APTT and TT). In summary, the SRHMGs had excellent anticoagulation properties.

In summary, the SRHMGs had a set of responses to changes in the environmental stimuli, such as pH, electronic field, and magnetic field. In addition, the SRHMGs showed good blood compatibility. As presented in Scheme 2, these microgels could be applied in controlled drug release, magnetic resonance imaging, biosensors, electronic devices, and tissue engineering.

4. CONCLUSIONS

SRHMGs were successfully prepared via a single-step cross-linking chemistry based on a 3F approach. The cross-linking reaction rapidly occurred during spray drying, and the functional hemicellulose microgels were made responsive to different external stimuli such as pH, electroactivity, magnetic field, and dual-stimuli (pH and electric field). Changes in the particle morphologies were observed due to the introduction of different functional groups, as confirmed by SEM. In addition, a spherical geometry of most of the particles was observed with an average diameter size in the range of 1−4 μm. Alterations in the surface chemistry and charge, as confirmed by IR, demonstrated that the functional materials were incorporated into and/or adsorbed onto the microparticles to provide stimuli response in different environments. Different oxidation states of AP were demonstrated using UV spectroscopy and CV, confirming the successful production of electroactive hemicellulose microgels ($H_{40}AP_{16}$ and $H_{40}AP_8PAA_4$). The $H_{40}PAA_8$ and $H_{40}AP_8PAA_4$ microgels showed reversible swelling behavior when the pH changed between 2.2 and 7.4 due to the pH sensitivity of PAA. In addition, the zeta potentials of the $H_{40}PAA_8$ and $H_{40}AP_8PAA_4$ microgels at pH 2.2−7.4 were in the range from 2 to −11 mV and from −0.5 to −15 mV, respectively, indicating their tunable charge properties. $H_{40}Fe_{16}$ exhibited a magnetic response in a magnetic field. Quantitative nanomechanical mapping revealed a broad distribution of Young's moduli (0−900 MPa) when the silicon tip indented PAA and AP/PAA. This result could be due to plastic deformation of the soft polymer, that is, PAA. Finally, these SRHMGs had prolonged clotting times and low hemolysis effects (<3%), which extends their applications to controlled drug release, magnetic resonance imaging, biosensors, electronic devices, and tissue engineering.

■ ASSOCIATED CONTENT

Supporting Information

The images, IR spectra, and TGA curves of stimuli-responsive hemicellulose microgels, proposed mechanism for the HCl doping of the electroactive hemicellulose microgels, cyclic voltammograms of AP in DMSO doped by three drops of 2 M HCl solution, molecular structure of AP segment in the microgels at various oxidation states. This material is available free of charge via the Internet at http://pubs.acs.org.

■ AUTHOR INFORMATION

Corresponding Author

*Phone:+46-8-790 8274. Fax: +46-8-20 8477. E-mail: aila@kth.se.

Author Contributions

[§]These authors contributed equally. The manuscript was written through contributions of all authors. All authors have given approval to the final version of the manuscript.

Funding

China Scholarship Council, the ERC Advanced Grant, PARADIGM (Grant No. 246776), the Major Program of the National Natural Science Foundation of China (Grant No. 51433007), and the Royal Institute of Technology.

Notes

The authors declare no competing financial interest.

■ ACKNOWLEDGMENTS

The authors are grateful to the China Scholarship Council, the ERC Advanced Grant, PARADIGM (Grant No. 246776), the Major Program of the National Natural Science Foundation of China (Grant No. 51433007), and the Royal Institute of Technology (KTH) for financial support of this work. Dr. H. Lu at the Dept of Applied Electrochemistry, School of Chemical Science in KTH is thanked for the kind support in the cyclic voltammetry testing. Mr. C. He at the College of Polymer Science and Engineering, Sichuan University, is thanked for his generous help in the blood compatibility measurements.

■ REFERENCES

(1) Walker, K. A.; Markoski, L. J.; Deeter, G. A.; Spilman, G. E.; Martin, D. C.; Moore, J. S. Cross-Linking Chemistry for High-Performance Polymer Networks. *Polymer* **1994**, *35*, 5012−5017.

(2) Billiet, S.; Hillewaere, X. K. D.; Teixeira, R. F. A.; Du Prez, F. E. Chemistry of Crosslinking Processes for Self-Healing Polymers. *Macromol. Rapid Commun.* **2013**, *34*, 290−309.

(3) Hennink, W. E.; van Nostrum, C. F. Novel Crosslinking Methods to Design Hydrogels. *Adv. Drug Delivery Rev.* **2002**, *54*, 13−36.

(4) Murphy, S. V.; Atala, A. 3D Bioprinting of Tissues and Organs. *Nat. Biotechnol.* **2014**, *32*, 773−785.

(5) Voepel, J.; Edlund, U.; Albertsson, A.-C. Alkenyl-Functionalized Precursors for Renewable Hydrogels Design. *J. Polym. Sci., Polym. Chem.* **2009**, *47*, 3595−3606.

(6) Li, Z.; Shen, J.; Ma, H.; Lu, X.; Shi, M.; Li, N.; Ye, M. Preparation and Characterization of pH- and Temperature-Responsive Nano-composite Double Network Hydrogels. *Mater. Sci. Eng., C* **2013**, *33*, 1951−1957.

(7) Bigand, V.; Pinel, C.; Perez, D. D. S.; Rataboul, F.; Huber, P.; Petit-Conil, M. Cationisation of Galactomannan and Xylan Hemicelluloses. *Carbohydr. Polym.* **2011**, *85*, 138−148.

(8) Ayoub, A.; Venditti, R. A.; Pawlak, J. J.; Salam, A.; Hubbe, M. A. Novel Hemicellulose-Chitosan Biosorbent for Water Desalination and Heavy Metal Removal. *ACS Sustainable Chem. Eng.* **2013**, *1*, 1102−1109.

(9) Zhao, W.; Glavas, L.; Odelius, K.; Edlund, U.; Albertsson, A.-C. A Robust Pathway to Electrically Conductive Hemicellulose Hydrogels with High and Controllable Swelling Behavior. *Polymer* **2014**, *55*, 2967−2976.

(10) Parasuraman, D.; Serpe, M. J. Poly(*N*-isopropylacrylamide) Microgels for Organic Dye Removal from Water. *ACS Appl. Mater. Interfaces* **2011**, *3*, 2732−2737.

(11) Xia, Y.; Gu, Y.; Zhou, X.; Xu, H.; Zhao, X.; Yaseen, M.; Lu, J. R. Controllable Stabilization of Poly(*N*-isopropylacrylamide)-Based Microgel Films through Biomimetic Mineralization of Calcium Carbonate. *Biomacromolecules* **2012**, *13*, 2299−2308.

DOI: 10.1021/am5084732
ACS Appl. Mater. Interfaces 2015, 7, 4202−4215

(12) Jia, X.; Yeo, Y.; Clifton, R. J.; Jiao, T.; Kohane, D. S.; Kobler, J. B.; Zeitels, S. M.; Langer, R. Hyaluronic Acid-Based Microgels and Microgel Networks for Vocal Fold Regeneration. *Biomacromolecules* **2006**, *7*, 3336−3344.
(13) Gao, Y.; Ahiabu, A.; Serpe, M. J. Controlled Drug Release from the Aggregation-Disaggregation Behavior of pH-Responsive Microgels. *ACS Appl. Mater. Interfaces* **2014**, *6*, 13749−13756.
(14) Schmidt, S.; Zeiser, M.; Hellweg, T.; Duschl, C.; Fery, A.; Moehwald, H. Adhesion and Mechanical Properties of PNIPAM Microgel Films and Their Potential Use as Switchable Cell Culture Substrates. *Adv. Funct. Mater.* **2010**, *20*, 3235−3243.
(15) Seliktar, D. Designing Cell-Compatible Hydrogels for Biomedical Applications. *Science* **2012**, *336*, 1124−1128.
(16) Kesselman, L. R. B.; Shinwary, S.; Selvaganapathy, P. R.; Hoare, T. Synthesis of Monodisperse, Covalently Cross-Linked, Degradable "Smart" Microgels Using Microfluidics. *Small* **2012**, *8*, 1092−1098.
(17) He, Y.; Chen, X.; Bi, S. Y.; Fu, W. G.; Shi, C. C.; Chen, L. Conferring pH-Sensitivity on Poly (Vinylidene Fluoride) Membrane by Poly (Acrylic Acid-co-Butyl Acrylate) Microgels. *React. Funct. Polym.* **2014**, *74*, 58−66.
(18) Dadsetan, M.; Taylor, K. E.; Yong, C.; Bajzer, Z.; Lu, L. C.; Yaszemski, M. J. Controlled Release of Doxorubicin from pH-Responsive Microgels. *Acta Biomater.* **2013**, *9*, 5438−5446.
(19) Fukae, K.; Terashima, T.; Sawamoto, M. Cation-Condensed Microgel-Core Star Polymers as Polycationic Nanocapsules for Molecular Capture and Release in Water. *Macromolecules* **2012**, *45*, 3377−3386.
(20) Gao, Y. F.; Serpe, M. J. Light-Induced Color Changes of Microgel-Based Etalons. *ACS Appl. Mater. Interfaces* **2014**, *6*, 8461−8466.
(21) Yue, M.; Hoshino, Y.; Ohshiro, Y.; Imamura, K.; Miura, Y. Temperature-Responsive Microgel Films as Reversible Carbon Dioxide Absorbents in Wet Environment. *Angew. Chem., Int. Ed.* **2014**, *53*, 2654−2657.
(22) Berger, S.; Zhang, H.; Pich, A. Microgel-Based Stimuli-Responsive Capsules. *Adv. Funct. Mater.* **2009**, *19*, 554−559.
(23) Wong, J. E.; Gaharwar, A. K.; Mueller-Schulte, D.; Bahadur, D.; Richtering, W. Dual-Stimuli Responsive PNiPAM Microgel Achieved via Layer-by-Layer Assembly: Magnetic and Thermoresponsive. *J. Colloid Interface Sci.* **2008**, *324*, 47−54.
(24) Hu, L.; Serpe, M. J. The Influence of Deposition Solution pH and Ionic Strength on the Quality of Poly(N-isopropylacrylamide) Microgel-Based Thin Films and Etalons. *ACS Appl. Mater. Interfaces* **2013**, *5*, 11977−11983.
(25) Li, H.; Luo, R. M.; Lam, K. Y. Multiphysics Modeling of Electrochemomechanically Smart Microgels Responsive to Coupled pH/Electric Stimuli. *Macromol. Biosci.* **2009**, *9*, 287−297.
(26) Bian, S. S.; Zheng, J.; Yang, W. L. Dual Stimuli-Responsive Microgels Based on Photolabile Crosslinker: Temperature Sensitivity and Light-Induced Degradation. *J. Polym. Sci., Polym. Chem.* **2014**, *52*, 1676−1685.
(27) Shi, S.; Wang, Q.; Wang, T.; Ren, S.; Gao, Y.; Wang, N. Thermo-, pH-, and Light-Responsive Poly(*N*-isopropylacrylamide-co-methacrylic acid)-Au Hybrid Microgels Prepared by the in Situ Reduction Method Based on Au-Thiol Chemistry. *J. Phys. Chem. B* **2014**, *118*, 7177−7186.
(28) Yuan, Z. C.; Wang, Y.; Chen, D. J. Preparation and Characterization of Thermo-, pH-, and Magnetic-Field-Responsive Organic/Inorganic Hybrid Microgels Based on Poly(ethylene glycol). *J. Mater. Sci.* **2014**, *49*, 3287−3296.
(29) Polotsky, A. A.; Plamper, F. A.; Borisov, O. V. Collapse-to-Swelling Transitions in pH- and Thermoresponsive Microgels in Aqueous Dispersions: The Thermodynamic Theory. *Macromolecules* **2013**, *46*, 8702−8709.
(30) Sollohub, K.; Cal, K. Spray Drying Technique: II. Current Applications in Pharmaceutical Technology. *J. Pharm. Sci.* **2010**, *99*, 587−597.
(31) Vehring, R. Pharmaceutical Particle Engineering via Spray Drying. *Pharm. Res.* **2008**, *25*, 999−1022.
(32) Esposito, E.; Roncarati, R.; Cortesi, R.; Cervellati, F.; Nastruzzi, C. Production of Eudragit Microparticles by Spray-Drying Technique: Influence of Experimental Parameters on Morphological and Dimensional Characteristics. *Pharm. Dev. Technol.* **2000**, *5*, 267−278.
(33) De Smet, R.; Verschuere, S.; Allais, L.; Leclercq, G.; Dierendonck, M.; De Geest, B. G.; Van Driessche, I.; Demoor, T.; Cuvelier, C. A. Spray-Dried Polyelectrolyte Microparticles in Oral Antigen Delivery: Stability, Biocompatibility, and Cellular Uptake. *Biomacromolecules* **2014**, *15*, 2301−2309.
(34) Ryberg, Y. Z.; Edlund, U.; Albertsson, A.-C. Innovative Approaches for Converting a Wood Hydrolysate to High-Quality Barrier Coatings. *ACS Appl. Mater. Interfaces* **2013**, *5*, 7748−7757.
(35) Arias, V.; O, K.; Albertsson, A.-C. Nano-stereocomplexation of Polylactide (PLA) Spheres by Spray Droplet Atomization. *Macromol. Rapid Commun.* **2014**, *35*, 1949−1953.
(36) Iwasaki, K. Production of a Functionally Graded Artificial Tooth Root by Unique Sequence of Processes. *Mater. Res. Innov.* **1997**, *1*, 180−187.
(37) Schnieders, J.; Gbureck, U.; Germershaus, O.; Kratz, M.; Jones, D. B.; Kissel, T. Ex Vivo Human Trabecular Bone Model for Biocompatibility Evaluation of Calcium Phosphate Composites Modified with Spray Dried Biodegradable Microspheres. *Adv. Healthcare Mater.* **2013**, *2*, 1361−1369.
(38) Jacobs, A.; Dahlman, O. Characterization of The Molar Masses of Hemicelluloses from Wood and Pulps Employing Size Exclusion Chromatography and Matrix-assisted Laser Desorption Ionization Time-of-Flight Mass Spectrometry. *Biomacromolecules* **2001**, *2*, 894−905.
(39) Huang, L.; Hu, J.; Lang, L.; Wang, X.; Zhang, P.; Jing, X.; Wang, X.; Chen, X.; Lelkes, P. I.; MacDiarmid, A. G.; Wei, Y. Synthesis and Characterization of Electroactive and Biodegradable ABA Block Copolymer of Polylactide and Aniline Pentamer. *Biomaterials* **2007**, *28*, 1741−1751.
(40) Derjaguin, B. V.; Muller, V. M.; Toporov, Y. P. Effect of Contact Deformations on The Adhesion of Particles. *J. Colloid Interface Sci.* **1975**, *53*, 314−326.
(41) Zhou, H.; Cheng, C.; Qin, H.; Ma, L.; He, C.; Nie, S.; Zhang, X.; Fu, Q.; Zhao, C. Self-Assembled 3D Biocompatible and Bioactive Layer at the Macro-interface via Graphene-Based Supermolecules. *Polym. Chem.* **2014**, *5*, 3563−3575.
(42) He, A.; Lei, B.; Cheng, C.; Li, S.; Ma, L.; Sun, S.; Zhao, C. Toward Safe, Efficient and Multifunctional 3D Blood-Contact Adsorbents Engineered by Biopolymers/Graphene Oxide Gels. *RSC Adv.* **2013**, *3*, 22120−22129.
(43) Wang, Y. X. J.; Hussain, S. M.; Krestin, G. P. Superparamagnetic Iron Oxide Contrast Agents: Physicochemical Characteristics and Applications in MR Imaging. *Eur. J. Radiol.* **2001**, *11*, 2319−2331.
(44) Zhao, W.; Glavas, L.; Odelius, K.; Edlund, U.; Albertsson, A.-C. Facile and Green Approach towards Electrically Conductive Hemicellulose Hydrogels with Tunable Conductivity and Swelling Behavior. *Chem. Mater.* **2014**, *26*, 4265−4273.
(45) Cao, X.; Prozorov, R.; Koltypin, Y.; Kataby, G.; Felner, I.; Gedanken, A. Synthesis of Pure Amorphous Fe_2O_3. *J. Mater. Res.* **1997**, *12*, 402−406.
(46) Glavas, L.; Odelius, K.; Albertsson, A.-C. Induced Redox Responsiveness and Electroactivity for Altering The Properties of Micelles without External Stimuli. *Soft Matter* **2014**, *10*, 4028−4036.
(47) Guo, B.; Finne-Wistrand, A.; Albertsson, A.-C. Molecular Architecture of Electroactive and Biodegradable Copolymers Composed of Polylactide and Carboxyl-Capped Aniline Trimer. *Biomacromolecules* **2010**, *11*, 855−863.
(48) Guo, B.; Finne-Wistrand, A.; Albertsson, A.-C. Enhanced Electrical Conductivity by Macromolecular Architecture: Hyperbranched Electroactive and Degradable Block Copolymers Based on Poly(epsilon-caprolactone) and Aniline Pentamer. *Macromolecules* **2010**, *43*, 4472−4480.
(49) Dubey, N. C.; Tripathi, B. P.; Stamm, M.; Ionov, L. Smart Core-Shell Microgel Support for Acetyl Coenzyme a Synthetase: A Step

DOI: 10.1021/am5084732
ACS Appl. Mater. Interfaces 2015, 7, 4202−4215

toward Efficient Synthesis of Polyketide-Based Drugs. *Biomacromolecules* **2014**, *15*, 2776−2783.
(50) Wu, L.; Zhang, J.; Watanabe, W. Physical and Chemical Stability of Drug Nanoparticles. *Adv. Drug Delivery Rev.* **2011**, *63*, 456−469.
(51) Luo, X.; Liu, S.; Zhou, J.; Zhang, L. In situ Synthesis of Fe_3O_4/Cellulose Microspheres with Magnetic-Induced Protein Delivery. *J. Mater. Chem.* **2009**, *19*, 3538−3545.
(52) Yap, S. F.; Adams, M.; Seville, J.; Zhang, Z. Understanding The Mechanical Properties of Single Micro-Particles and Their Compaction Behaviour. *China Particuol.* **2006**, *4*, 35−40.
(53) Goldberg, M.; Langer, R.; Jia, X. Nanostructured Materials for Applications in Drug Delivery and Tissue Engineering. *J. Biomater. Sci., Polym. Ed.* **2007**, *18*, 241−268.
(54) Nugroho, R. W. N.; Roy, P. K.; Odelius, K.; Albertsson, A.-C. Crosslinked PVAL Nanofibers with Enhanced Long-Term Stability Prepared by Single-Step Electrospinning. *Polym. Adv. Technol.* **2013**, *24*, 421−429.
(55) Platz, D.; Tholen, E. A.; Pesen, D.; Haviland, D. B. Intermodulation Atomic Force Microscopy. *Appl. Phys. Lett.* **2008**, *92*, 1−3.
(56) Qin, H.; Sun, C.; He, C.; Wang, D.; Cheng, C.; Nie, S.; Sun, S.; Zhao, C. High Efficient Protocol for The Modification of Polyethersulfone Membranes with Anticoagulant and Antifouling Properties via in situ Cross-Linked Copolymerization. *J. Membr. Sci.* **2014**, *468*, 172−183.
(57) Xiao, Y.; Fan, Y.; Wang, W.; Gu, H.; Zhou, N.; Shen, J. Novel GO-COO-β-CD/CA Inclusion: Its Blood Compatibility, Antibacterial Property and Drug Delivery. *Drug Delivery* **2014**, *21*, 362−369.
(58) Leung, L. L. K. Perioperative Evaluation of Bleeding Diathesis. *Hematology (Am. Soc. Hematol. Educ. Program)* **2006**, 457−461.
(59) Nie, S.; Qin, H.; Cheng, C.; Zhao, W.; Sun, S.; Su, B.; Zhao, C.; Gu, Z. Blood Activation and Compatibility on Single-Molecular-Layer Biointerfaces. *J. Mater. Chem. B* **2014**, *2*, 4911−4921.

DOI: 10.1021/am5084732
ACS Appl. Mater. Interfaces 2015, 7, 4202−4215